Supplemental Material:

Magnetic damping properties of single-crystalline $Co_{55}Mn_{18}Ga_{27}$ and $Co_{50}Mn_{18}Ga_{32}$ films

Jia-Rui Chen(陈家瑞)[1], Yu-Ting Gong(龚钰婷)[2], Xian-Yang Lu(陆显扬)[2, *], Chen-Yu Zhang(张晨宇)[3], Yong Hu(胡勇)[3, *], Ming-Zhi Wang(王铭志)[4], Zhong Shi(时钟)[4], Shuai Fu(付帅)[1], Hong-Ling Cai(蔡宏灵)[1, 5], Ruo-Bai Liu(刘若柏)[1], Yuan Yuan(袁源)[1], Yu Lu(卢羽)[1], Tian-Yu Liu(刘天宇)[1], Biao You(游彪)[1, 5], Yong-Bing Xu(徐永兵)[2], Jun Du(杜军)[1, 5, *]

[1]*National Laboratory of Solid State Microstructures and Department of Physics, Nanjing University, Nanjing 210093, P. R. China*

[2]*York-Nanjing Joint Center (YNJC) for Spintronics and Nano-Engineering, School of Electronic Science and Engineering, Nanjing University, Nanjing 210093, P. R. China*

[3]*College of Sciences, Northeastern University, Shenyang 110819, P. R. China*

[4]*School of Physics Science and Engineering, Tongji University, Shanghai 200092, P. R. China*

[5]*Collaborative Innovation Center of Advanced Microstructures, Nanjing 210093, P. R. China*

S1. FFT spectra at various external magnetic fields

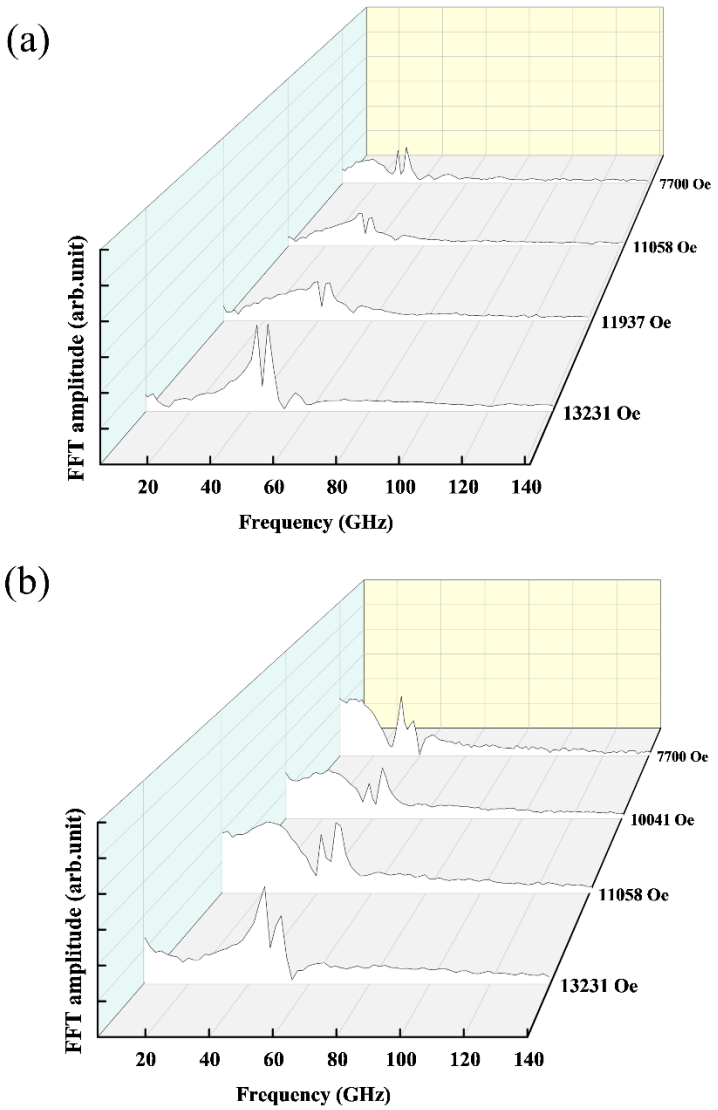

Figure S1. FFT spectra corresponding to the TRMOKE signals shown in Fig. 3(a) and Fig. 3(b) in the main text for CMG1 (a) and CMG 2 (b), respectively.

S2. Comparison of frequencies obtained by TRMOKE and FFT

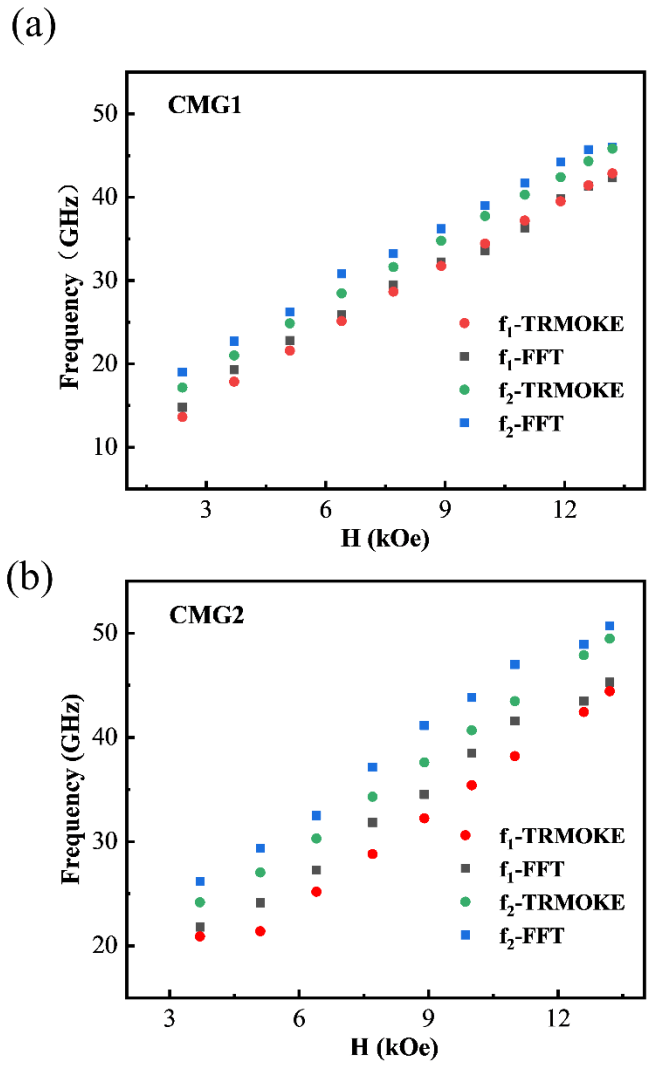

Figure S2. f_1 (Kittle mode) and f_2 (PSSW mode) obtained by directly fitting with the TRMOKE signals and by FFT for CMG1 (a) and CMG 2 (b), respectively.

S3. Exclusion of Damon-Eshbach (DE) mode

Note that the femtosecond laser wavelength and the probe size of our TRMOKE setup is 800 nm, 250 μm, respectively. Firstly, the excitation of surface DE mode requires that the ferromagnetic metal layer thickness is much larger than the penetration depth of 15-20 nm for the 800 nm femtosecond laser pulses [1]. This implies that the DE mode can not be easily excited in the present CMG films with the thickness of only 50 nm. Secondly, in addition to the Kittel mode, if the high-frequency signal belongs to DE mode, its frequency should satisfy the equation [2] as

$$f_{DE}^2 = f_{Kittel}^2 + (\frac{\gamma}{2\pi})^2 \frac{H_x M_s^2}{4}[1 - \exp(-2k_{DE}L)], \quad \text{(S1)}$$

where k_{DE}, γ, H_x, M_s, L and f_{Kittel} are the wave vector, gyromagnetic ratio, in-plane applied magnetic field, saturation magnetization, film thickness and the frequency of the Kittel mode, respectively. According to this equation and H_x = 13231 Oe, the estimated values of k_{DE} are ~ 10 nm^{-1} and 2 nm^{-1} and the corresponding wavelengths are ~ 0.6 nm and ~ 3 nm for CMG1 and CMG2, respectively. Such small wavelengths are impossible to be detected with a probe size in diameter of 250 μm in our measurements. Similar discussion can be seen in Ref. [3] in this Supplementary Material. Therefore, the high-frequency mode for CMG1 or CMG2 is not a DE mode.

S4. First-Principles Calculations

The microscopically structural and magnetic properties for Co-Mn-Ga full Heusler alloys with stoichiometric ($Co_{50}Mn_{25}Ga_{25}$) and Mn-deficient compositions ($Co_{56.25}Mn_{18.75}Ga_{25}$ and $Co_{50}Mn_{18.75}Ga_{31.25}$) are numerically studied by implementing the first-principles calculations. The calculations have been performed based on the density functional theory (DFT) using the Vienna Ab-initio Simulation Package (VASP) [4-6]. The interaction of ions and electrons is described by the Projector-Augmented Wave (PAW) method [7,8], and the Generalized Gradient Approximation (GGA) based on the Perdew-Burke-Ernzerhof (PEB) formulation is used to deal with the exchange-correlation energy [9]. The electronic configurations are set by $3d^74s^2$ (Co), $3d^64s^1$ (Mn) and $4s^24p^1$ (Ga), respectively. The plane wave cutoff energy is 520 eV. A Monkhorst-pack grid is employed to sample the Brillouin zone [10], and the number of **k**-points is

selected as 6×6×6 to provide a similar level of the total energy convergence as that of the cutoff energy. The Wigner-Seitz radii are 1.25, 1.37 and 1.53 Å for Co, Mn and Ga, respectively. All structures have been relaxed using the conjugate gradient algorithm and both the atomic positions and lattice parameters have been optimized. The convergence criteria for the electronic self-consistent iteration is set to 10^{-7} eV and the ionic relaxation continued until the maximum force on each atom is less than 0.001 eV/Å. The calculation results and corresponding discussion can be seen in the following.

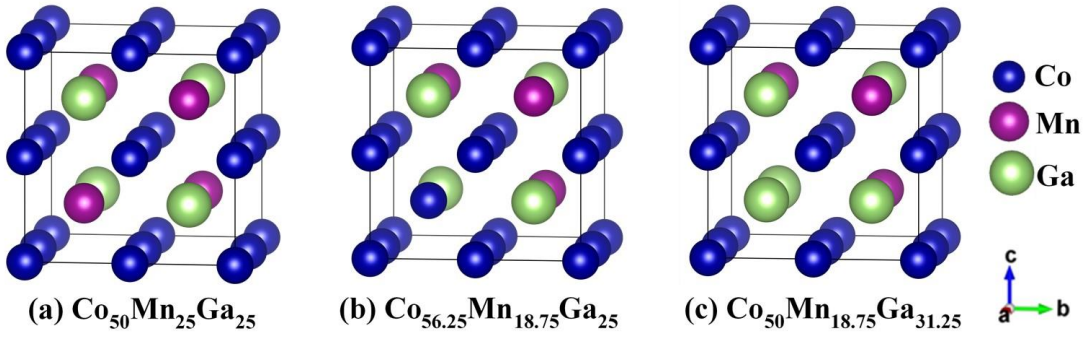

Figure S3. Schematic view of the crystal structures of Co-Mn-Ga full Heusler alloys with selected chemical structures. (a) Stoichiometric compound, and off-stoichiometric compounds where the same Mn atom is replaced by (b) Co and (c) Ga, respectively.

Table S1. Equilibrium lattice parameters and total/spin-projected magnetic moments of Co-Mn-Ga full Heusler alloys with different chemical structures.

Samples	a (Å)	b (Å)	c (Å)	m_{Co} (μ_B)	m_{Mn} (μ_B)	m_{Ga} (μ_B)	m_{Total} (μ_B)
$Co_{50}Mn_{25}Ga_{25}$	5.716	5.716	5.716	0.718	2.772	-0.082	4.125
$Co_{56.25}Mn_{18.75}Ga_{25}$	5.716	5.716	5.716	1.007	2.816	-0.081	4.331
$Co_{50}Mn_{18.75}Ga_{31.25}$	5.736	5.736	5.736	0.591	2.936	-0.063	3.305

Figure S3 shows the crystal structures of unit cell for Co-Mn-Ga full Heusler alloys, which consists of four face-centered cubic (FCC) sublattices. The unit cell has FCC lattices with four atoms as basis at A = (0 0 0), B = (1/4 1/4 1/4), C = (1/2 1/2 1/2), and D = (3/4 3/4 3/4) in Wyckoff coordinates. For the stoichiometric $Co_{50}Mn_{25}Ga_{25}$ compound, the A and C sites are occupied by Co, the B site by Mn, and the D site by Ga. Therefore, each Mn or Ga atom has eight Co atoms as first neighbors sitting in an octahedral symmetry position, while each Co atom has four Mn atoms and four Ga atoms as first neighbors and the symmetry of the crystal is reduced to the tetrahedral one. The results of the equilibrium lattice parameters are listed in Table S1, and show that the cubic structure remains. The lattice constant is invariant for $Co_{50}Mn_{25}Ga_{25}$ and $Co_{56.25}Mn_{18.75}Ga_{25}$ compounds while slightly increases for $Co_{50}Mn_{18.75}Ga_{31.25}$ compound, probably due to the larger radius of Ga atom than that of Mn atom. Remarkably, the regular Co atoms occupying two different sublattices are chemically equivalent as the environment of the second one but rotated by 90º. Although the regular Co atoms are sitting on the second-neighbor positions, their interactions are important to explain the magnetic properties of these compounds as we will show in the following.

The results of the equilibrium total and spin-projected magnetic moments are also listed in Table S1, and the total magnetic moment increases by 5% from 4.125 μ_B to 4.331 μ_B for substitution of a Co atom for a Mn atom, on the contrary, a 20% reduction of the total magnetic moment to 3.305 μ_B is observed when the Mn atom is replaced by a Ga atom. For the spin-projected magnetic moments, the magnetic moment value per atom of Mn is the largest, and their value slightly increases from the stoichiometric $Co_{50}Mn_{25}Ga_{25}$ compound (2.772 μ_B) to the off-stoichiometric $Co_{56.25}Mn_{18.75}Ga_{25}$ compound (2.816 μ_B), and to the off-stoichiometric $Co_{50}Mn_{18.75}Ga_{31.25}$ compound (2.936 μ_B). The Co atoms are ferromagnetically coupled to Mn, while the Ga atoms are antiferromagnetically coupled to Mn. The induced magnetic moments of Ga are small. The total and spin-projected magnetic moment values for the stoichiometric $Co_{50}Mn_{25}Ga_{25}$ compound agree with the calculations of Galanakis *et al*. who studied the $Co_{50}Mn_{25}Ga_{25}$ compound using the full-potential screened Korringa-Kohn-

Rostoker Green's function method [11]. Different from the results obtained from the compounds with different *sp* atoms, the difference of the total magnetic moments between the Co-Mn-Ga compounds with different chemical structures mainly depends on Co.

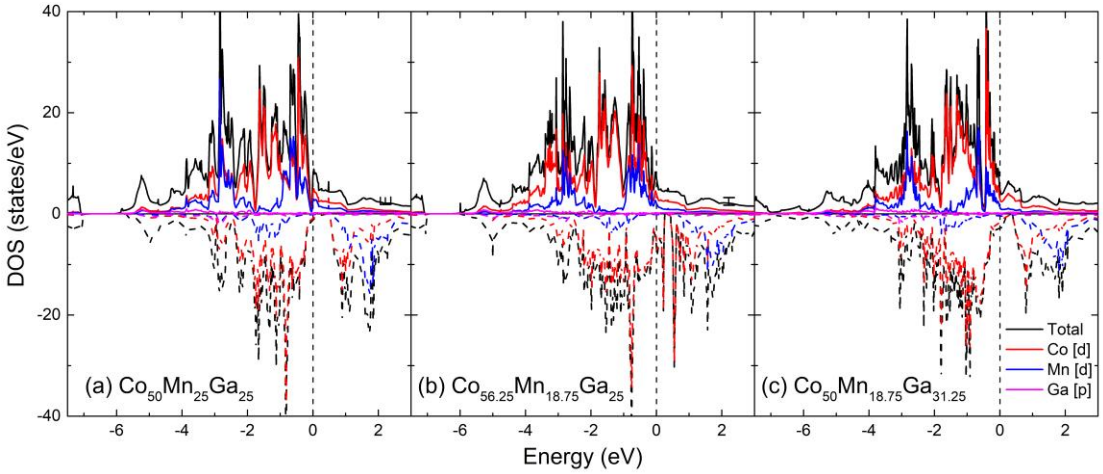

Figure S4. The total and spin-projected density of states (DOS) of Co-Mn-Ga full Heusler alloys with selected chemical structures. Solid and dashed curves indicate the spin-up and spin-down results, and the *d* states are given for Co and Mn, while the *p* state for Ga.

In order to interpret the magnetic moment behaviors in the three compounds, the total and spin-projected density of states (DOS) are calculated and depicted in Figure S4, where the results of Co *d* states, Mn *d* states and Ga *p* states are presented. The valence band extends 6 eV below the Fermi level and the spin-up DOS shows a large peak just below the Fermi level for these compounds. On the contrary, the Fermi level falls within a region of very small spin-down DOS, in particular, the state of Fermi level is at the left edge of the gap for $Co_{50}Mn_{25}Ga_{25}$ compound, while the states of Fermi level become well below the gap for the off-stoichiometric compounds. The similar results of DOS in stoichiometric compound have also been reported [11, 12]. For the spin-projected DOS, it is remarkable that the Co *d* state curves best approach to those of the total DOS curves, evidencing that the Co magnetic properties play a dominant role on establishing the total magnetic properties of different compounds. Galanakis *et al.* [11] discussed that the formation of not a real gap at the Fermi level in the spin-down DOS may be ascribed from the lift of the band degeneracy probably caused by spin-orbit

coupling to destroy the indirect gap.

Several groups [12-14] have presented that the magnetic properties can be also well understood in terms of the hybridization between Co and Mn atoms, and the indirect exchange of the Mn *d* electrons through the *sp* atom (Ga). Remarkably, the considerably large hybridization between Co and Mn is observed in $Co_{56.25}Mn_{18.75}Ga_{25}$ compound, and the excess Co atoms occupying the Mn sites are also ferromagnetically coupled to the regular Co atoms and the surrounding Mn atoms. Therefore, both the Co magnetic moment and the total magnetic moment are enhanced, which has been evidenced by Galanakis *et al*. [11] through discussing the hybridizations between two different Co atoms and between Co and Mn atoms in $Co_{50}Mn_{25}Ge_{25}$. On the contrary, the substitution of Ga for Mn may weaken the hybridizations between magnetic atoms, leading to the decrease of Co magnetic moment and thus to the decrease of total magnetic moment, although the magnetic moment of Mn is weakly influenced.

Finally, based on the results listed in Table S1 and presented in Figure S4, the ratios of DOS value at the Fermi level [$D(E_F)$] to m_{Total} are calculated by 8.539/4.125 = 2.070 for $Co_{50}Mn_{25}Ga_{25}$ compound, 12.632/4.331 = 2.917 for $Co_{56.25}Mn_{18.75}Ga_{25}$ compound, and 10.529/3.305 = 3.186 for $Co_{50}Mn_{18.75}Ga_{31.25}$ compound, respectively, and the intrinsic damping constant α_0 is proportional to the $D(E_F)/m_{Total}$ ratio [15]. Thus, the damping α_0 can be estimated by $\alpha_0(Co_{50}Mn_{25}Ga_{25}) < \alpha_0(Co_{56.25}Mn_{18.75}Ga_{25}) < \alpha_0(Co_{50}Mn_{18.75}Ga_{31.25})$. The damping results agree with the experimental findings. It is interpreted that the increase of damping in $Co_{56.25}Mn_{18.75}Ga_{25}$ compound as compared to $Co_{50}Mn_{25}Ga_{25}$ compound mainly originates from the enhancement of $D(E_F)$, and the highly increase of damping in $Co_{50}Mn_{18.75}Ga_{31.25}$ compound is attributed to the contributions of both the increase of $D(E_F)$ and the shrink of m_{Total}.

References

[1] Zhu W, Zhu Z, Li D, Wu G, Xi L, Jin Q, and Zhang Z 2019 *J. Magn. Magn. Mater.* **479**, 179

[2] Walowski J, Kaufmann M D, Lenk B, Hamann C, McCord J, and ünzenberg M M 2008 *J. Phys. D: Appl. Phys.* **41**, 164016

[3] Lu X, Atkinson L J, Kuerbanjiang B, Liu B, Li G, Wang Y, Wang J, Ruan X, Wu J, Evans R F L, Lazarov V K, Chantrell R W, and Xu Y 2019 *Appl. Phys. Lett.* **114**, 192406

[4] Hafner J 2000 *Acta Mater.* **48**, 71

[5] Kresse G and Furthmüller 1996 J *Phys. Rev. B* **54**, 11169

[6] Kresse G and Furthmüller J 1996 *Comput. Mater. Sci.* **6**, 15

[7] Perdew J P and Wang Y 1992 *Phys. Rev. B* **45**, 13244

[8] Blöchl P E 1994 *Phys. Rev. B* **50**, 17953

[9] Perdew J P, Burke K, and Ernzerhof M 1996 *Phys. Rev. Lett*. **77**, 3865

[10] Monkhorst H J and Pack J D 1976 *Phys. Rev. B* **13**, 5188

[11] Galanakis I, Dederichs P H, and Papanikolaou N 2002 *Phys. Rev. B* **66**, 174429

[12] Kübler J, Williams A R, and Sommers C B 1983 *Phys. Rev. B* **28**, 1745

[13] Galanakis I, Dederichs P H, and Papanikolaou N 2002 *Phys. Rev. B* **66**, 134428

[14] Reitz J R and Stearns M B 1979 *J. Appl. Phys*. **50**, 2066

[15] Mizukami S, Wu F, Sakuma A, Walowski J, Watanabe D, Kubota T, Zhang X, Naganuma H, Oogane M, Ando Y, and Miyazaki T 2011 *Phys. Rev. Lett*. **106**, 117201